



P1

X-RAY HIGH RESOLUTION IMAGING CCD CAMERA BASED ON A THIN SCINTILLATOR SCREEN

J. Touš¹, K. Blažek¹, L. Pína², B. Sopko³

¹*Crytur spol. s r.o., Palackého 175, Turnov CZ-511 01, Czech Republic*

²*Faculty of Nuclear Sciences and Physical Engineering, Czech Technical University, V Holešovičkách 2, Praha 8 CZ-18000, Czech Republic*

³*Faculty of Mechanical Engineering, Czech Technical University, Technická 4, Praha 6 CZ-16607, Czech Republic*
tous@crytur.cz

A high-resolution CCD X-ray camera based on YAG:Ce or LuAG:Ce thin scintillators is presented. The high resolution in low energy X-ray radiation is proved on several objects. The achieved spatial resolution of the images is better than 1 micron. The objects used for imaging are grids and small animals with parts of several microns in dimension. The high-resolution imaging system can be used for different types of ionizing radiation (X-Ray, electron, UV, and VUV) for non-destructive micro-radiography and synchrotron beam inspection.

Introduction

The spatial resolution of an X-ray and ionizing radiation imaging system is one of its most important parameters in X-ray non-destructive micro-radiography and radiation beam inspection. The imaging systems are mostly based on two-dimensional position-sensitive detectors (PSD). There are many different types of PSD detectors with each having its advantages and disadvantages [1]. X-ray micro-radiography is an X-ray imaging method well known from a number of medical and biological applications related to the imaging of very small objects. The sample is irradiated with X-rays with energies sufficient for penetrating the object and being detected with a fine resolution X-ray position-sensitive detector. Different parts of the sample usually have different integral (different integral absorption lengths can be caused by different materials or different thicknesses) attenuation lengths for X-rays of given energy and therefore the intensity of detected X-rays depends on the properties of the sample materials.

The presented high resolution imaging system is a combination of a high sensitive digital CCD camera and an optical system with a thin scintillator imaging screen. The screen is the YAG:Ce ($Y_3Al_5O_{12}$) or LuAG:Ce ($Lu_3Al_5O_{12}$) inorganic scintillator. High quality industrial YAG:Ce and LuAG:Ce single crystals were prepared by the Czochralski method [2] at Crytur. These materials have the advantages in the mechanical and chemical stability and the non-hygroscopicity. The imaging scintillator screen is optically transparent. The emission wavelength of YAG:Ce and LuAG:Ce is 550 nm and 535 nm, respectively.

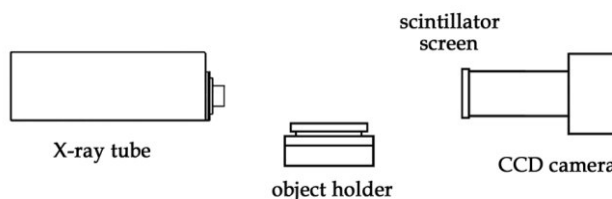


Figure 1. Experimental setup.

Experiments

The scheme of the experimental setup is shown in Figure 1. The scintillator was placed in the focused object plane of the optics. In the experiments, the scintillators have the shape of a round plate with diameter of 19 mm and thickness of 20 μm . Several objects were placed in proximity to the imaging screen in order to keep the smearing effect caused by the X-ray focal spot size as low as possible. To achieve high resolution, a microfocus X-ray tube was used. The temperature of the camera was stabilized by recirculating water cooling chiller. The resulting images were processed via dark background subtraction and flat field correction.

Results and discussion

Figure 2 presents an image of a golden grid made of wires which have a size of about 10 microns. The image was taken by using the LuAG:Ce 20 μm screen. The effective pixel size of the CCD camera used was 0.74 μm . The X-ray microfocus source was operated at 40 kV/2mA. The image acquisition time was 5 s and the averaging was performed with samples of 25 images.

It shows that the resolution of the imaging system is in the order of micrometers. The line profile of one grid wire is shown in Figure 3. The profile is compared with the geometric profile of the grid wire, which has trapezoidal shape with a base of 10.7 μm and top 6.8 μm wide (measured in an SEM image of the grid).

The optical properties of YAG:Ce and LuAG:Ce materials allow to achieve the very high spatial resolution of 1 micrometer, which is about ten times higher than standard X-ray imaging CCD cameras (standard X-ray imaging CCD cameras have pixel size from 10 to 24 μm , also due to charge capacity and use mainly non-transparent phosphors). The spatial resolution of the screen depends on screen thickness, photon energy and the depth of absorption of the photon. An

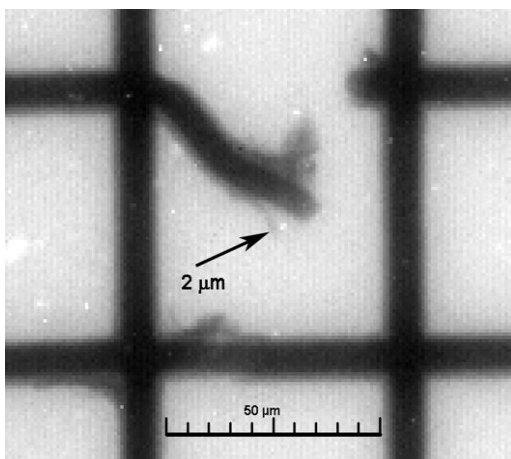


Figure 2. Radiography of a gold-grid taken by using LuAG:Ce thin screen.

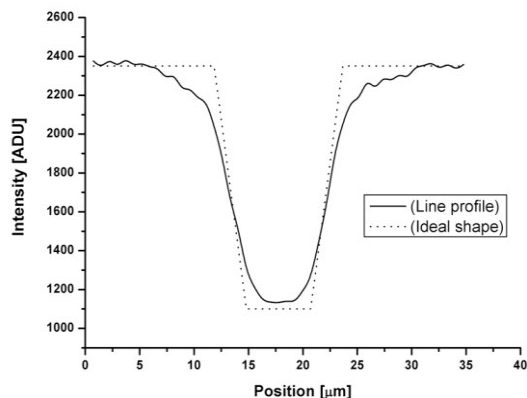


Figure 3. Line profile of the grid wire.

optical system using a magnifying lens was used to transfer the scintillator screen image to the CCD image area surface.

Several biological samples were studied in the next experiments. Here only *Drosophila* is presented. The image is shown in Figure 4 with the grayscales indicating the transparency of the sample.

The images were taken by the CCD camera in the same setup as the images of the grid, using a YAG:Ce 20 μm screen and a magnifying lenses. The acquisition time was set to 20 s.

The zoom image showing selected details of the fly's leg in Figure 5 demonstrates that a resolution of about several μm is achievable by the used imaging system. The effective pixel size of the system is about 0.65 μm.

The intensity of the light generated by LuAG:Ce is about 1,51 times the value of YAG:Ce. The light was detected by the CCD and averaged in a squared ROI of 200 x 200 pixels. The LuAG:Ce single crystal is more dense compared to YAG:Ce (density: 6.73 to 4.57 g.cm⁻³) and the X-rays are absorbed stronger by LuAG (1.7 times more of X-ray radiation (photons) is absorbed in the range between 1 and 40 keV), as can be seen in Figure 6. Attenuation coefficients are taken from [3].

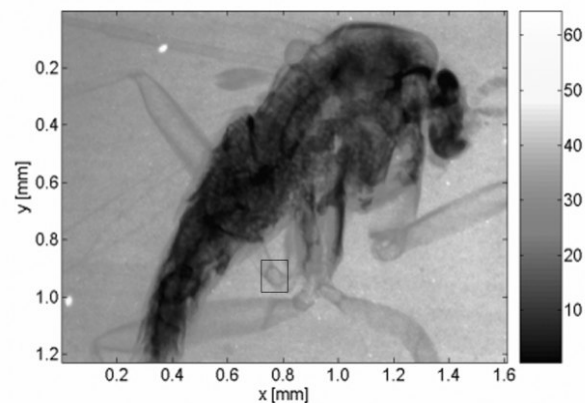


Figure 4. Microradiography of the body of *Drosophila melanogaster*.

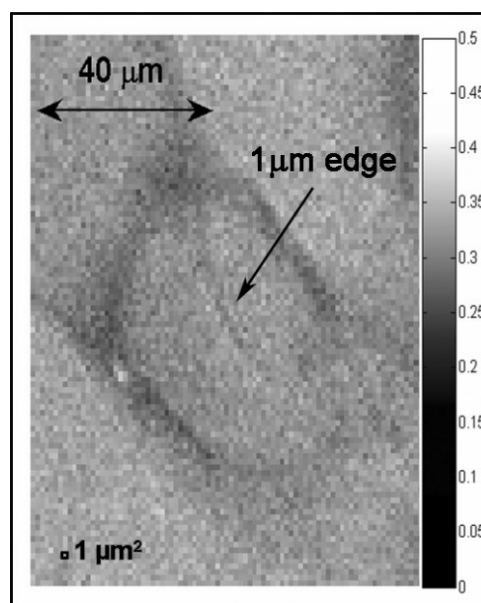


Figure 5. Microradiography of *Drosophila melanogaster* – a detail of the leg.

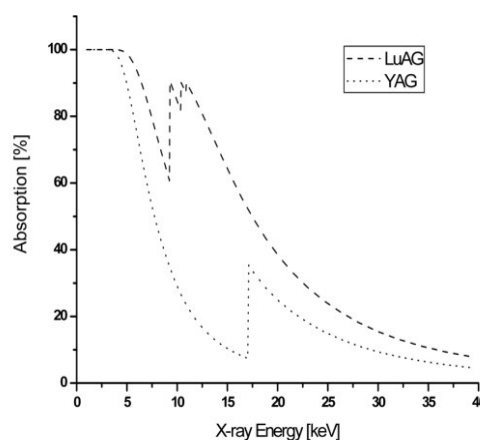


Figure 6. Absorption of X-ray radiation in 20 microns thick layer of YAG and LuAG [3].



Conclusion

In the experimental setup presented, a high resolution imaging system based on CCD camera with lenses and precisely manufactured YAG:Ce and LuAG:Ce single crystal screens was used for X-ray micro-radiography.

The mean absorption depth of X-ray radiation in the scintillator depends on photon energy and the material. The YAG:Ce and LuAG:Ce screens are optically transparent so the image of interaction points is easily transferred to the CCD. However, the advantage of the material transparency decreases with the thickness of the imaging plate. If the scintillator is thinner, the mean absorption depth is lower and the created image is sharper due to less blurring of the image due to less lateral spread of the scintillation photons. Hence, the thinner the imaging plate is, the better is the resolution achieved in the image. On the other hand, the detection efficiency decreases with scintillator thickness.

The experiments proved that the YAG:Ce and LuAG:Ce screens are suitable for imaging with high spatial resolution. The submicrometer spatial resolution using synchrotron radiation has been already achieved [4]. The

resolution of the presented imaging system is about one micrometer.

The LuAG:Ce screen has higher conversion efficiency than the YAG:Ce screen, so that the signal to noise ratio of the image is better.

References

1. van Eijk, Carel W. E., Inorganic scintillators in medical imaging; *Phys. Med. Biol.* **47** (2002) R85-R106.
2. Brandle, C.D., Czochralski growth of oxides, *J. Crystal Growth*, **264** (2004) 593-604.
3. X-Ray Form Factor, Attenuation, And Scattering Tables, <http://physics.nist.gov/>.
4. Koch, A., X-ray imaging with submicrometer resolution employing transparent luminescent screens, *J. Opt. Soc. Am. A*/Vol. **15**, No. 7/July 1998, 1940-1951.

Acknowledgements

This work was supported by the grant of the Ministry of industry and trade of the Czech Republic no. FT-TA/100.

P2

PHOTOIONIZATION FOR BENCHMARK STUDIES IN TRANSITION-METAL CATALYSIS

Detlef Schröder

Institute of Organic Chemistry and Biochemistry, Czech Academy of Sciences, Flemingovo nám. 2, 16610 Prague 6, Czech Republic

The concepts for employing photoionization studies with synchrotron radiation for benchmark studies in transition-metal chemistry are outlined briefly. As an illustration, the exemplarily case of trimethoxy-vanadium oxide is presented, where photoionization data essentially helped to establish the entire thermochemistry of $\text{OV}(\text{OCH}_3)_3$ from the neutral compound to the quasi-terminal fragments VO^+ and VOH^+ in the gaseous phase.

1. Introduction

Experiments with VUV photons (7–60 eV) stemming from synchrotron sources are of outmost importance as a linkage between modern and advanced experimentation in chemistry and physics on the one hand and the more and more improving theoretical tools on the basis of quantum mechanics. Nowadays, one may in fact state that ab initio theoretical studies of a problem in main-group chemistry may be more adequate, more accurate, require less personal and infrastructure and are faster and cheaper than conventional experimentation.

Despite the enormous progress of quantum theory within the last two decades, these methods need testing and benchmarking for keeping standards as well as to warrant a continuous improvement. Moreover, the high standards of accuracy have meanwhile only been reached for main-group elements, whereas transition-metal compounds form a considerably more challenging task.

This is the point of linkage at which experiments with well-resolved VUV photons from a synchrotron source provide a junction between experiment and theory by means of the highly accurate determination of atomic or molecular quantities (such as ionization energies, vibrational levels, excited states etc.) or - in fortunate cases - even allow the determination of activation barriers of chemical reactions. While in main-group chemistry, such experiments thus present a test for existing theoretical tools, in transition-metal research the benchmarks derived from synchrotron experiments essentially stimulate the progress in the development of new methods.

2. Methods for the delivery of benchmark data

Instead of detailed descriptions of the beamlines or the experimental end-stations used at the synchrotron facilities, only the general concepts for the establishment of benchmark data will be introduced. With the availability of tunable VUV photons from a synchrotron source, various chemical compounds can be excited and/or ionized. If samples are used which are sufficiently volatile in ultra-high vacuum at ambient temperatures (typically up to a few hundreds °C), photoionization by synchrotron radiation can be combined with mass spectrometric techniques, which ensures a highly sensitive detection on a single-event counting basis. As an example, consider a molecular species M having an ionization energy of 10.0 eV. Below the ioniza-

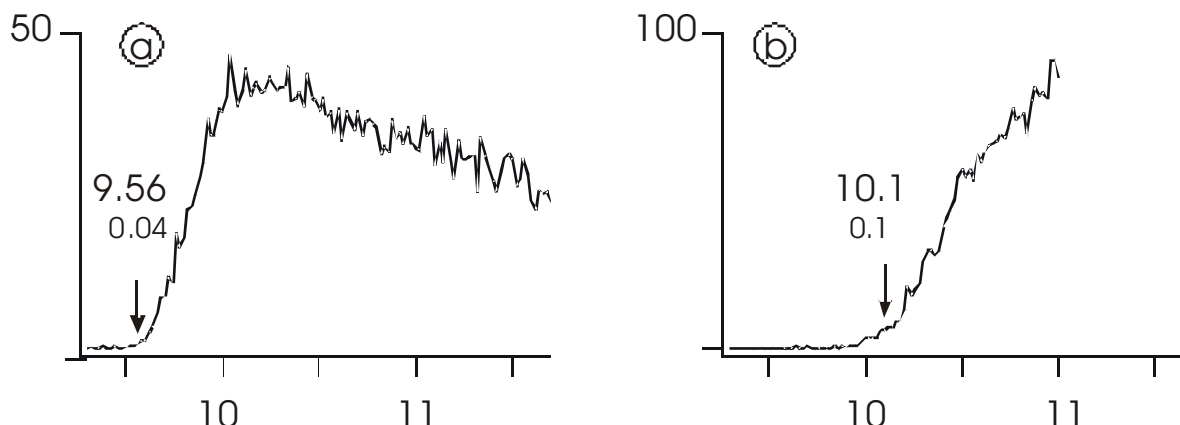


Figure 1. Photoionization yields of (a) the molecular ion $OV(OCH_3)_3^+$ and (b) the fragment ion $HOV(OCH_3)_2^+$ as a function of the energy of the photons used to ionise neutral, gaseous $HOV(OCH_3)_2^+$ [5].

tion threshold, the few M^+ cations being formed can be attributed to impact from cosmic irradiation inside the apparatus (typical count rate $0.03 - 0.1 \text{ s}^{-1}$). Slightly below the ionization threshold, Rydberg states of the neutral molecule, M^* , can be formed which may eventually autoionize to the molecular ion M^+ , but the cross section of these processes is usually very low. If the photon energy reaches the very ionization threshold, however, the M^+ signal increases very rapidly to a plateau regime with typically several 10^4 counts per second. When the analyzer of the mass spectrometer is fixed on the mass-to-charge ratio of the molecular ion M^+ , the photoionization threshold of M can thus be determined by monitoring M^+ as a function of the wavelength (and the flux) of the ionizing photons. The typical precision amounts to about $\pm 0.005 \text{ eV}$ for atomic and $\pm 0.03 \text{ eV}$ for molecular species [1]; double photoionization to dications has less favourable threshold characteristics and thus at best $\pm 0.1 \text{ eV}$ [2,3]. Thresholds for dissociative ionization are broadened by Franck-Condon effects and thus also only precise by $\pm 0.1 \text{ eV}$ at best [1].

3. Case study: Ion thermochemistry of trimethoxovanadium oxide $OV(OCH_3)_3$

Vanadium-oxide catalysts play a very important role in a number of large-scale processes such as in the oxidation of methanol to formaldehyde, the oxidative dehydrogenation of ethylbenzene, or the industrial production of maleic anhydride. A key problem in these processes, both partial oxidations, is the minimisation of competing combustion processes eventually leading to CO_x . In this respect, the knowledge of the elementary steps of such oxidation reactions is of prime importance as it can help to increase the yields of the desired products, thereby reducing the amounts of byproducts, waste, and heat production.

One way to achieve detailed insight into the elementary steps of catalytic processes are gas-phase studies of small model systems, both by experiment and modern quantum theory. These extensive efforts, on the experimental as well as the computational sides, need some dedicated benchmarks for evaluation of the performance of the different methods. In this respect, photoionization experiments with synchrotron radiation can provide essential

information which cannot be achieved by any other means. As an example, we refer to the trimethoxovanadium oxide, $OV(OCH_3)_3$, which can be regarded as a model system for C-H bond activations by high-valent transition-metal oxides [4].

Figure 1 shows the photoion yields of the molecular ion $OV(OCH_3)_3^+$ (Figure 1a) and the primary fragment $HOV(OCH_3)_2^+$ (Figure 1b), where the latter is accompanied with the loss of formaldehyde and hence represents an example of an oxidation reaction. Analysis of the photoion yields reveals thresholds of $(9.56 \pm 0.04) \text{ eV}$ for the photoionization of the neutral compound to the cation and $(10.1 \pm 0.1) \text{ eV}$ for dissociative photoionization to $HOV(OCH_3)_2^+$ [5]. Both values provide accurate benchmarks for the calibration of theoretical methods, in that the former describes the energy demand for removal of one electron from the vanadium (V) compound, thus resembling defect formation in the solid state, and the latter turns out to be not due a thermochemical limit imposed by the exit channel but rather represents the height of the activation barrier for C-H bond activation.

The usefulness of the synchrotron data is demonstrated by the success of subsequent work [6], in which starting from neutral $OV(OCH_3)_3$ the combined expertise of experiment and theory could be used to establish the thermochemistry of trimethoxovanadium oxide from the bulk, neutral compound to the quasi-terminal fragments VO^+ and VOH^+ , respectively (Figure 2).

4. Conclusions

The above example as well as related work [7,8] demonstrate that photoionization experiments using synchrotron radiation provide accurate reference data for the reliable testing and calibration of other experimental methods and for the critical evaluation of modern theoretical approaches. In this respect, the exploitation of synchrotron radiation for essays in transition-metal chemistry is just in its infancy and thus likely to essentially contribute to the future success in this field.



Figure 2. Ion thermochemistry from the molecular ion $\text{OV}(\text{OCH}_3)_3^+$ to the quasi-terminal fragments VO^+ and VOH^+ .

References

1. D. Schröder, J. Loos, H. Schwarz, R. Thissen, O. Dutuit, *J. Phys. Chem. A* **108**, (2004), 9931.
2. J. Roithová, D. Schröder, J. Loos, H. Schwarz, H.-C. Jankowiak, R. Berger, R. Thissen, O. Dutuit, *J. Chem. Phys.* **122**, (2005), 094306.
3. J. Roithová, J. Žabka, D. Ascenzi, P. Franceschi, C.L. Ricketts, D. Schröder, *Chem. Phys. Lett.* **423**, (2006), 254.
4. M. Engeser, D. Schröder, H. Schwarz, *Chem. Eur. J.* **11**, (2005), 5975.
5. D. Schröder, J. Loos, M. Engeser, H. Schwarz, C. Jankowiak, R. Berger, R. Thissen, O. Dutuit, J. Döbler, J. Sauer, *Inorg. Chem.* **43**, (2004), 1976.
6. D. Schröder, M. Engeser, H. Schwarz, E. C. E. Rosenthal, J. Döbler, J. Sauer, *Inorg. Chem.* **45**, (2006), 6235.
7. D. Schröder, J. Loos, H. Schwarz, R. Thissen, O. Dutuit, *Inorg. Chem.* **40**, (2001), 3161.
8. Á. Révész, Cs. I. Pongor, A. Bodi, B. Sztáray, T. Baer, *Organometallics*, **25**, (2006), 6061.

Acknowledgements

This work was supported by the Czech Academy of Sciences (Z40550506).

DESIRS A SOLEIL - STANOVENÍ IONIZAČNÍCH ENERGIÍ

P. Milko¹, J. Roithová^{1,2}, O. Perlík¹, D. Schröder¹

¹Ústav organické chemie a biochemie, AV ČR, 166 10 Praha 6, Česká republika

²Ústav organické chemie, Přírodovědecká fakulta, Karlova univerzita v Praze, 128 43 Praha 2, Česká republika
petr.milko@uochb.cas.cz

Úvod

Vícenásobně nabitě molekuly hrají významnou roli v atmosférické chemii a také astrochemii, kde jsou zkoumány kvůli jejich roli při tvorbě vyšších polycyklických uhlovodíků [1]. Předchozí studie se zabývaly uhlovodíky bez heteroatomů, naše studie se mimo to zaměřuje na uhlovodíky obsahující dusík a zahrnuje také srovnání s předchozími daty změřenými pro homocyklické uhlovodíky. Veškerá naše měření jsou prováděna v plynné fázi, kde se podmínky nejvíce blíží podmínkám, ve kterých se tyto vícenásobně nabitě částice mohou v přírodě vyskytovat.

Teorie

Fotoionizace molekul slouží k získání velmi přesných hodnot ionizačních energií molekul v plynné fázi. Výhodou této metody oproti jiným je znalost přesné energie, která je poskytována molekulám během ionizace. Jako příklad jiné metody může sloužit „charge-stripping“ hmotnostní spektrometrie, která k ionizaci používá srážky s neutrálními molekulami - např. dusíkem a při níž se měří rozdíl kinetických energií monokationtů před kolizí a dikationtů po kolizi. Rozdíl kinetických energií se přepočítává na ionizační energie pomocí kalibrace. Špatná kalibrace může vést k nepřesným výsledkům a z následné revize kalibrace logicky vyplývá nutnost opravit všechny výsledky na ní založené [2].

Fotoionizace do prvního i do druhého stupně je popsána Wannierovým zákonem [3-6]. V případě ionizace do prvního stupně zákon předpokládá závislost relativní intenzity iontu na energii fotonu ve formě tzv. skokové funkce. Tento předpoklad je dobře splněn v oblasti do dvou elektronvoltů nad ionizačním prahem. Pro ionizaci do druhého stupně Wannierův zákon předpokládá již lineární závislost relativní intenzity iontu na ionizační energii, tež platnou do 2 eV nad ionizační prah.

Experiment

Jako zdroj synchrotronního záření slouží zařízení SOLEIL v Saint-Aubin [7]. Tento synchrotron operuje s energií elektronového svazku 2.75 GeV a poskytuje záření o vlnové délce v rozsahu od infračervené oblasti do tvrdé rentgenové oblasti.

K měření ionizačních energií je využívána fotonová linka s názvem DESIRS. DESIRS je napojena na undulátor, jenž pracuje v oblasti spektra 30 až 250 nm. Uvedená oblast odpovídá přibližně operační oblasti 5–40 eV, která pokrývá předpokládaný rozsah prvních a druhých ionizačních energií organických molekul.

Synchrotronové záření je přivedeno do zdroje hmotnostního spektrometru ve kterém je zkoumaný plynný vzorek při tlaku cca $1 \cdot 10^{-4}$ Pa. Vlastní hmotnostní spektrometr má konfiguraci QQQ, kde Q znamená kvadrupól a O octopól. Pokud fotony obsahují dostatek energie k ionizaci vzorku na detektoru hmotnostního spektrometru zaznamáme signál nabitých částic. Pomocí kvadrupolového hmotnostního detektoru můžeme podle hmoty sledovat námi studované ionty a potlačit vliv pozadí. Výsledkem je pak závislost intenzity požadované hmoty na energii přiváděných fotonů, z které se podle Wannierova zákona pomocí interpolace určí hodnota ionizační energie.

Pro interpretaci a srovnávání výsledků z fotoionizačního experimentu lze použít kvantově chemické výpočty. Studované systémy jsou náročné na výpočetní čas při použití *ab initio* metod, proto je zvolena metoda hustotního funkcionálu B3LYP s bazí 6-311++G(2d,p) obsahující polarizační a difuzní funkce.

Výsledky a diskuze

V prvním kroku je nutné provést kalibraci energetické stupnice. Provádíme ji s pomocí vzácných plynů, jejichž ionizační energie jsou velmi přesně známy.

Jako první vzorek byl použit 2,4,6-trimethylpyridin $C_8H_{11}N$ (Schéma 1), u nějž bylo provedeno srovnání první ionizační energie s daty z literatury.

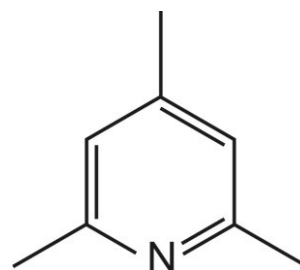
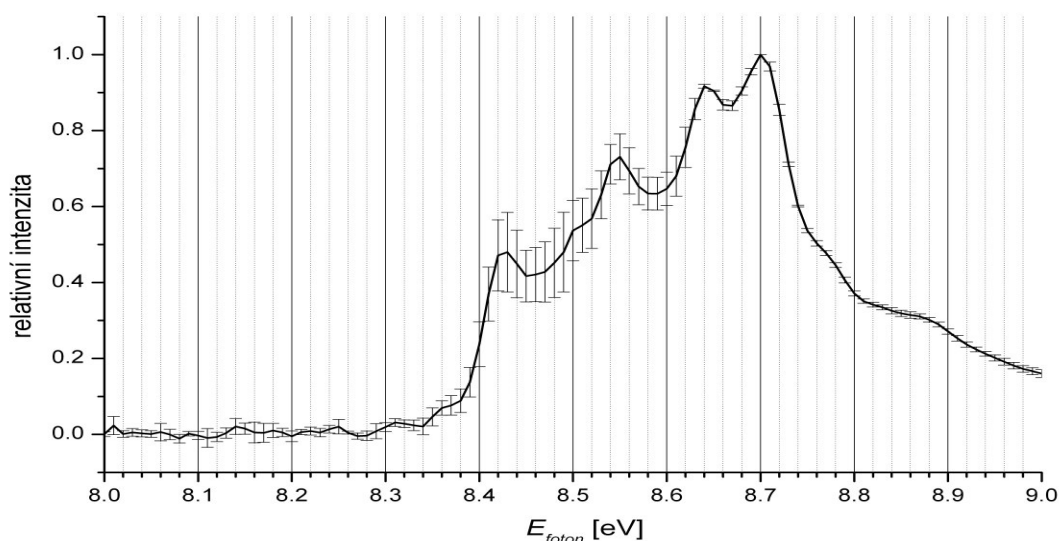


Schéma 1. 2,4,6-trimethylpyridin ($C_8H_{11}N$).

Obrázek 1 ukazuje závislost relativní intenzity $C_8H_{11}N^+$ na energii fotonů E_{foton} . Závislost je opravena na intezitu fotonů a energetická stupnice je kalibrována měřeními ionizačních energií vzácných plynů.

Z analýzy grafické závislosti vychází hodnota první ionizační energie 8.38 ± 0.05 eV. Vypočtená hodnota ionizační energie je stanovena na 8.43 eV. Obě hodnoty jsou si blízké, avšak výrazně se liší od dříve publikované hodnoty 8.9 ± 0.1 eV pro 2,4,6-trimethylpyridin [8].



Obrázek 1. Závislost relativní intenzity $C_8H_{11}N^+$ na energii fotonů E_{foton} . Závislost je očištěna od vlivu intenzity fotonů a energetická stupnice je kalibrována.

Závěr

První výsledky experimentu potvrzují úspěšnou aplikaci synchrotronního záření v chemickém výzkumu, konkrétně v oblasti studující ionizační energie. Vysoký energetický potenciál a specifické vlastnosti synchrotronového záření slibují do budoucna přesné stanovení ionizačních energií látek, pro které byly ionizační energie doposud obtížně dostupné, zvláště pak u dvojnásobné ionizace. Stejně tak umožňuje ověření předchozích dosažených výsledků pro důležité sloučeniny, které jsou používány jako standardy.

8. B.G. Ramsey, F.A. Walker, *J. Am. Chem. Soc.*, **96**, (1974), 3314.

Poděkování

Práce byla podpořena záměrem AV ČR (Z40550506) a záměrem Ministerstva školství České republiky (MSM00 21620857).

Literatura

1. J. Roithová, D. Schröder, *J. Am. Chem. Soc.*, **128**, (2006), 4208.
2. J. Roithová, D. Schröder, J. Loos, H. Schwarz, H.-Ch. Jankowiak, R. Berger, *J. Chem. Phys.*, **122**, (2005), 094306.
3. G.H. Wannier, *Phys. Rev.*, **90**, (1953), 817.
4. S. Geltman, *Phys. Rev.*, **102**, (1956), 171.
5. U. Fano, *Rep. Prog. Phys.*, **46**, (1983), 97.
6. M. S. Lubell, *Z. Phys. D-At., Mol. Clusters*, **30**, (1994), 79.
7. <http://www.synchrotron-soleil.fr/portal/page/portal/Accueil>

CRYSTALLIZATION STUDY OF HIGH PLANTS PHOTOSYSTEM II AND CHLOROSOMAL BACTERIOCHLOROPHYLL C AGGREGATES

Tatyana Prudnikova¹, José A. Gavira³, Pavlína Řezáčová⁴, Michal Kutý^{1,2}, František Vácha^{1,5}, Jakub Pšenčík⁶, Juan M. García-Ruiz³ and Ivana Kutá Smatanová^{1,2}

¹Institute of Physical Biology USB CB, Zamek 136, 373 33 Nove Hradky, Czech Republic

²Institute of Systems Biology and Ecology AS CR Zamek 136, 373 33 Nove Hradky, Czech Republic

³Laboratorio de Estudios Cristalografico, Edf. Lopez Neira, P.T. Ciencias de la Salud, Avenida del Conocimiento, s/n, 18100 Armilla, Granada, Spain

⁴Institute of Molecular Genetics AS CR, Flemingovo n. 2, 16637 Prague, Czech Republic

⁵Biological Centre IPMB AS CR, Branisovska 31, 370 05 Ceske Budejovice, Czech Republic

⁶Charles University, Faculty of Mathematics and Physics, Ke Karlovu 3, CZ-121 16, Czech Republic

Photosynthesis realized by photosystem II (PS II) uses light energy to couple the formation of molecular oxygen to the fixation of carbon dioxide. It consists of four membrane-internal subunits (D1, D2, CP43, CP47), several smaller internal membrane (including PsbE and PsbF, constituting *cyt b-559*) and three external subunits (PsbQ, PsbP, PsbO in green algae and higher plants). PS II is located in the thylakoid membrane of higher plants, algae and cyanobacteria.

Chlorosomes are the main light harvesting complexes of green photosynthetic bacteria. Typical chlorosome is an ellipsoidal body (100-200 nm x 20-50 nm) which consists of bacteriochlorophyll (*c*, *d* or *e*) molecules, carotenoids (chlorobactene), very small amount of quinones (menaquinone-7), lipids (monogalactosyl diglyceride) and proteins. The main difference from other light harvesting complexes is that the main pigments aren't associated with protein and self-assemble into aggregates.

The aim of our work was based on using advanced counter-diffusion and standard vapor-diffusion methods, to observe capability of individual precipitants to influence the crystals growth.

Using advanced counter-diffusion method and common vapor diffusion techniques we have tested the influence of several salt additives from Hampton Research screening test (Fe, Ca, Ba, Mg, Ca, Mn, Cd, Cu, Co, Cs, Zn, Y, Ni and Sr), detergents (DM, C₁₂E₈), buffers with different pH (MES, HEPES, Tris, KH₂PO₄, pH 6.0-8.0), and cryoprotectants (PEG with several molecular mass, glycerol, MPD) to find suitable conditions to produce single crystals of diffraction quality. Crystals of hexagonal shape and needles obtained from different conditions were measured at the synchrotrons DESY, Hamburg (Germany),



Figure 1. Crystals of Higher Plants Photosystem II.

EMBL, Grenoble (France) and diffractometer Granada (Spain).

1. K. N. Ferreira, T. M. Iverson, K. Maghlaoui, J. Barber, S. Iwata (2004), *Science*, 303, 1831-1838.
2. I. Kuta-Smatanova, J.A. Gavira, P. Rezacova, F. Vacha, J.M. Garcia-Ruiz (2005), *Acta Cryst.*, A61, 147.
3. F. Vácha, J. Pšenčík, M. Kutý, M. Durchan and P. Šiffel: *Photosynthesis Research*, 84 (2005) 297.
4. V. I. Prokhorenko, D. B. Steensgaard, A. R. Holzwarth: *Biophysical Journal*, 85 (2003) 3173-3186.

This work is supported by grants NSM6007665808 and LC06010 of the Ministry of Education of Czech Republic and Institutional research concept AVOZ60870520 of Academy of Science of Czech Republic.



P5

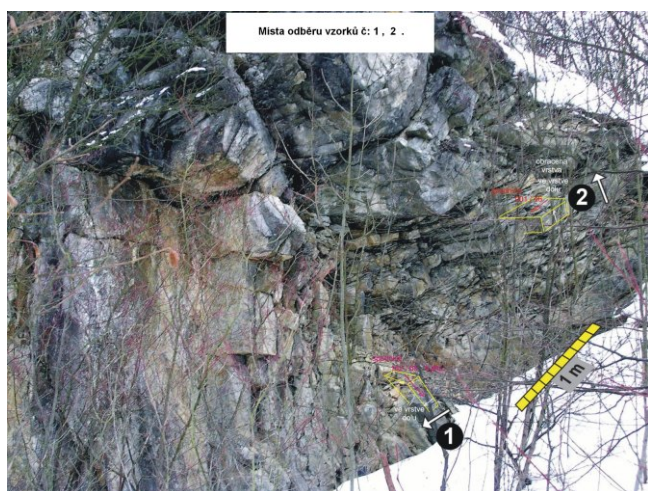
TEXTURY VÁPENCOVÝCH VRSTEV

J. Marek¹, J. Hladil²

¹Jaderná fakulta ČVUT, Katedra inženýrství pevných látek, Trojanova 13, CZ-120 00 Praha 2,

²J. Hladil: Geologický ústav ČAV, Rozvojevá 269, CZ-165 00, Praha 6-Lysolaje

K rentgenografickému difrakčnímu rozboru byly dodány Geologický ústavem ČAV, vzorky vápence z lomu „Na Škrábků“ lokality Choteč. Vzorky byly odebrány z vápencové zahnuté vrstvy (Obr. 1).



Obrázek 1.

Odběry z míst 1 a 2 byly provedeny ve tvaru krychli o straně délky cca 2 cm. Krychle byly dále rozřezány na destičky tloušťky cca 3.5 mm. (obr. 2)

Difraktogramy byly provedeny na práškovém goniometru Siemens, záření Co-anody.

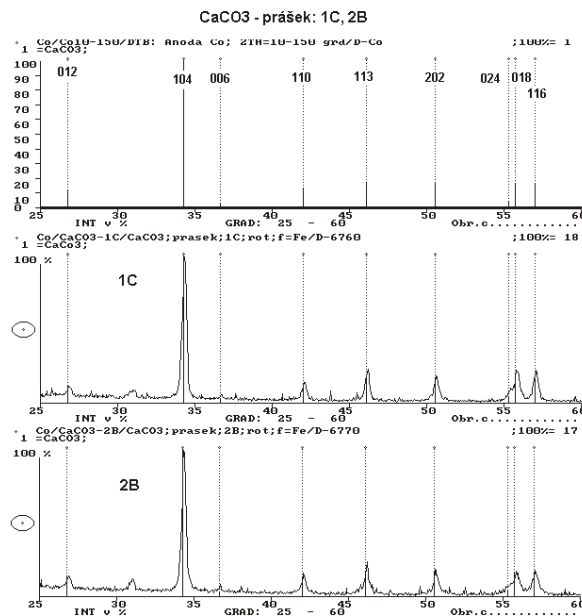
Difraktogramy rozemletých vzorků jsou uvedeny na obr. 3, intenzivní difrakce jsou identifikovány dle databáze PDF Calcite, File: 5-586.



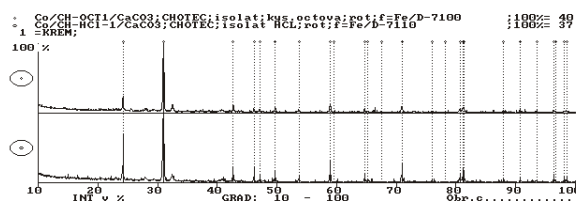
Obrázek 2.

Pro identifikaci dalších složek bylo větší množství materiálu rozpuštěno jednak v kyselině octové, jednak v kyselině chlorovodíkové HCl. Práškové difraktogramy isolátů jsou uvedeny na obr. 4.

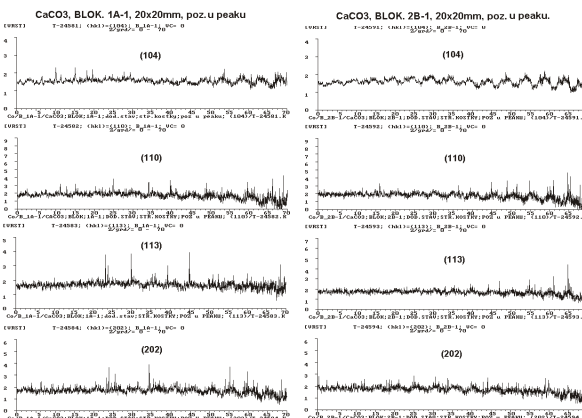
Intenzivní difrakce jsou identifikovány dle databáze PDF Křemen, File 5-498.



Obrázek 3.



Obrázek 4.



Obrázek 5.

Na difraccích Calcitu (104), (110), (113), (202) (viz obr. 3) byly provedeny texturogramy odříznutých destiček, na texturním goniometru Siemens, (anoda Co), jejichž rozvinuté spirálové záznamy jsou uvedeny na obr.5.

Z uvedených texturogramů je patrna velmi nízká přednostní orientace měřených vzorků.

Výzkum byl podpořen grantem MSM 6840770040.

P6

UTILIZATION OF SYNCHROTRON RADIATION FOR IN-SITU DIFFUSION STUDIES

M. Meduňa¹, O. Caha¹, G. Bauer², G. Mussler³, D. Grützmacher³

¹*Institute of Condensed Matter Physics, Masaryk University Brno, Czech Republic*

²*Institut für Halbleiterphysik, J Kepler Universität, Linz, Austria*

³*Institute of Bio- and Nanosystems, Forschungszentrum Jülich GmbH, Jülich, Germany*
mjme@physics.muni.cz

New devices in electronic and optoelectronic applications, often designed in nanometer scale, are typically subjected to a large thermal load during its production, processing and operation. On the contrary the thermal properties of the new materials used are usually not well known and they result in fast degradation processes at high temperatures. In these cases the in-situ diffraction techniques are very appropriate for detection of temporal structural changes inside the investigated structure.

In our case, we concentrate on studies of interdiffusion in SiGe electronic devices, which find applications in CMOS technologies, quantum cascade emitters and quantum dot structures. Unfortunately, there are only few experimental data on interdiffusion available in literature. Sufficient set of parameters describing interdiffusion in Ge rich SiGe alloys is still completely missing with reliable precision [1].

We have investigated diffusion properties of strain compensated SiGe multiple quantum well (MQW) structures grown by molecular beam epitaxy. The series of structures with various average Ge contents were studied in-situ by means of reciprocal space mapping of X-ray diffraction or reflectivity using synchrotron radiation (ESRF). Since the temporal evolution of structural changes is usually very fast within the large dynamical range of intensities and close to a

detection limit, a high intensity flux was required for in-situ annealing measurements. The annealing at high temperatures requires appropriate ambient conditions, for instance high vacuum, which was realized inside evacuated Be dome chamber allowing proper scattering conditions.

In our experiment, we have found that critical temperatures, where the interdiffusion starts to be evident, is observed in the range from 600 °C to 700 °C for Ge rich SiGe alloys with $x_{\text{Ge}}=70$ and 90 % and from 700 °C to 800 °C for Si rich alloys with $x_{\text{Ge}}=25$ and 50 % [2]. The MQW period in different sample series varied in the range from 5 nm to 30 nm. The layer thicknesses and Ge contents obtained from simulations of diffraction patterns allowed us to determine the diffusion coefficients for various temperatures and several average Ge contents in the MQW.

1. D. B. Aubertine & P. C. McIntyre, *J. Appl. Phys.*, **97**, (2005), 13531.
2. M. Meduňa, J. Novák, G. Bauer, C.V. Falub, & D. Grützmacher, *phys. stat. sol. (a)*, (2008), in print.

P7

DIFUZNÍ RTG ROZPTYL NA POLOVODIČOVÝCH KVANTOVÝCH TEČKÁCH

T. Čechal

Ústav fyziky pevných látek, Masarykova univerzita Brno

Tato práce se zabývá analýzou struktury SiGe kvantových teček připravených metodou LPE na Si(001) substrátu. V nedávné době byly vyvinuty metody umožňující zjištění chemického složení a deformačního pole v těchto kvantových tečkách založené na analýze rtg difrakčního obrazce pořízeného v GID geometrii. Cílem práce je zobecnit tyto metody na případ klasické koplánární geometrie. Jedním z možných přístupů je vytvoření vhodného zjednodušeného

strukturního modelu kvantové tečky a následné fitování naměřeného difrakčního obrazce. Vhodnost navrženého strukturního modelu je testována pokusným fitováním difrakčního obrazce získaného "brute-force" simulací a následně je tento strukturní model použit k fitování skutečných experimentálních dat.



SYNTHESIS OF TITANATE NANOTUBES: INFLUENCE OF TiO₂ MODIFICATION ON CRYSTALLINE STRUCTURE AND MORPHOLOGY

D. Králová¹, M. Šlouf^{1,2}, R. Kužel³

¹*Institute of Macromolecular Chemistry, Academy of Sciences of the Czech Republic, Heyrovského nam. 2, 162 06 Praha 6, Czech Republic*

²*Member of Consortium for Research of Nanostructured and Crosslinked Polymeric Materials (CRNCPM)*

³*Department of Electronic Structures, Faculty of Mathematics and Physics, Charles University, 121 16 Praha 2, Ke Karlovu 5, Czech Republic
kralova@imc.cas.cz*

This work is focused on preparation of titanate nanotubes (Ti-NT) from various modifications of TiO₂. Different source micro/nanopowders of TiO₂ yielded Ti-NT with similar sizes, shapes and structures. Residual TiO₂ particles in final Ti-NT suspensions were eliminated by modification of preparation procedure. Morphology and crystalline structure of both source TiO₂ and final Ti-NT were investigated by means of electron microscopy, electron diffraction and X-ray diffraction.

Introduction

Recently discovered titanate nanotubes [1] attracted special attention in the nanomaterial research due to their novel unique crystalline structure and morphology [2-4] as well as the mechanism of their formation [5-7]. The nanoparticles are basically rolled sheets of titanate. Their outer diameter is about 10 nm and their length varies from 100 nm to 1 μm. Nanotubes are obtained by simple hydrothermal process without using of templates. Due to their high aspect ratio, titanate nanotubes (Ti-NT) have potential use as nanofillers in polymer composites, similarly to carbon nanotubes. They may not exhibit as unique properties as carbon nanotubes, but they are highly uniform, their fabrication is simple, inexpensive and highly reproducible.

In our previous work we developed an isolation method yielding non-destructed and non-merged nanotubes from aqueous solution in gram-scale amounts [8]. Problem of our isolation method consisted in that we had always obtained a mixture of Ti-NT and anatase or rutile as proved by powder X-ray diffraction. Main objective of this work was to refine the synthesis so that we get rid of residual TiO₂. Moreover, we wanted to compare the differences among syntheses starting from various TiO₂ crystal sizes and modifications. The morphology of both source TiO₂ and final Ti-NT was investigated by means of scanning and transmission electron microscopy. The crystalline structure was studied by X-ray and electron diffraction.

Experimental

Synthesis of titanate nanotubes. Starting TiO₂ modifications included: technical powder (Riedel-de Haën, Sigma-Aldrich), anatase TiO₂ nanopowder (99,8%; Aldrich), rutile micropowder (99,9%, Aldrich) or rutile nanopowder (99,9%, Aldrich). In the following text, the TiO₂ powders are denoted as follows: technical powder -

microanatase (mA), anataseTiO₂ nanopowder – nanoanatase (nA), rutile micropowder – microrutile (mR), rutile nanopowder – nanorutile (nR). Titanate nanotubes (Ti-NT) were synthesized by hydrothermal synthesis as reported in our previous work [8], but several modifications were made. Firstly, three different concentrations of TiO₂ technical powder were used: 6 g, 1 g and 0.1 g TiO₂ per 100 ml of reactive mixture. Secondly, reaction time was prolonged to 48 hours. Thirdly, Ti-NT were synthesized from mA, nA, mR or nR (where mA, nA, mR and nR are defined above; initial concentration of TiO₂ = 0.1 g; reaction time = 48 hours).

Scanning electron microscopy. All Ti-NT (or TiO₂) aqueous suspensions were sonicated 1 min just before final preparation for electron microscopy. A drop of Ti-NT/TiO₂ suspension was deposited on bulk carbon support and left to evaporate. After complete evaporation, the carbon support with investigated particles was transferred into scanning electron microscope (SEM) Quanta 200 FEG (FEI, Czech Republic). The specimens were observed as they were in low-vacuum mode using accelerating voltage 30 kV.

Transmission electron microscopy and electron diffraction. The specimens were sonicated as described in the previous paragraph. A droplet of the sonicated suspension was deposited on a thin, transparent carbon film, left to evaporate and then inspected in a transmission electron microscope (TEM; Tecnai G² Spirit 120, FEI, Czech Republic). The specimens were studied in both bright field (conventional TEM/BF) and selected-area electron diffraction (TEM/ED) modes at 120 kV.

Powder X-ray diffraction. Powder X-ray diffraction (PXRD) measurements of whole patterns were performed mainly on XRD7 (FPM-Seifert) diffractometer with monochromator in the diffracted beam. The PXRD results were compared with simulated powder diffraction patterns (calculated by program PowderCell, [9]) and experimental ED diffraction patterns (processed by program Process Diffraction, [10]).

Results and discussion

Hydrothermal synthesis of titanate nanotubes can be schematically described by very simple reaction: TiO₂ Ti-NT, which usually takes place at elevated temperatures > 100 °C and high concentrations of NaOH. In this study, the first variable parameter of the syntheses was the initial

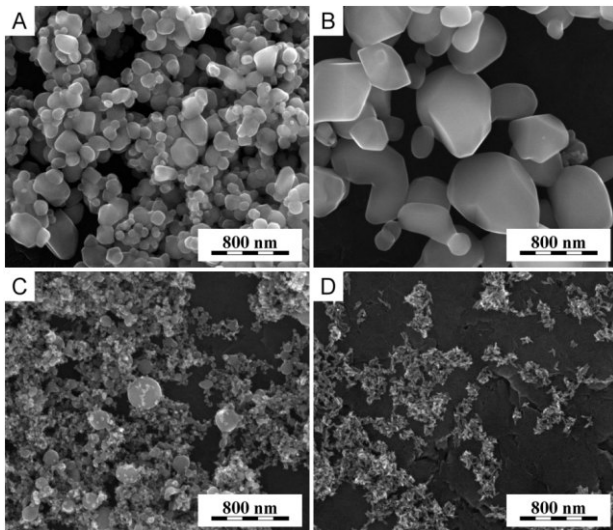


Figure 1. Various TiO_2 particles for the syntheses: (a) microparticles of anatase (mA), (b) microparticles of rutile (mR), (c) nanoparticles of anatase (nA) and (d) nanoparticles of rutile (nR).

concentration of source TiO_2 powders. The next two variables were average particle size and crystalline modification of source TiO_2 powders. The size of TiO_2 particles was characterized by SEM as shown in Fig. 1. Size of particles was very different (mA: 500nm - 100nm; mR: 1 μm - 300nm; nA: 300nm - 20nm; nR: 90nm - 20nm). Absolute purity of anatase (Fig. 1a,c) and rutile (Fig. 1b,d) modifications was proved by both electron and X-ray diffraction.

PXRD patterns in figure 2 illustrate influence of initial concentration TiO_2 on purity of synthesized Ti-NT. The reaction time was prolonged from 20 h (ref. [8]) to 48 h (this work). If 6 g of mA was used, the reaction mixture was so dense that after 20 h that stirring was almost impossible, which probably caused that reaction did not proceed homogeneously in the whole volume. Consequently, PXRD pattern showed mixture of Ti-NT and anatase. Similar behavior was observed also for 1 g of mA. As low concentration as 0.1 g of mA per 100 ml of reaction mixture was necessary to obtain suspension, which could be homogeneously mixed for whole 48 hours. PXRD patterns in Fig. 2 confirmed gradual decrease of anatase concentration in the final Ti-NT suspensions from high content of residual anatase (Fig. 2b) to pure Ti-NT (Fig. 2d).

TEM/BF micrographs and TEM/ED patterns in Fig. 3 show influence of TiO_2 crystallite size and modification on Ti-NT morphology and crystalline structure. TEM results proved that all crystal modifications and sizes of source TiO_2 (Fig. 1) can be used for synthesis of Ti-NT (Fig. 3, BF micrographs). Closer inspection of both TEM and SEM micrographs suggested that the finest and thinnest nanotubes were synthesized from powder of nanorutile, nR.

Electron diffraction (Fig. 3 and Fig. 4) re-confirmed that all *single nanotubes of Ti-NT* had the same structure, with three characteristic diffractions ($2\theta = 24, 28$ and 48° for $\text{CuK}\alpha$), which is in agreement with our previous work [8]. However, powder X-ray diffraction suggested that the crystalline structure of Ti-NT prepared from micropowders (Fig. 4a,b) differed from the structure of

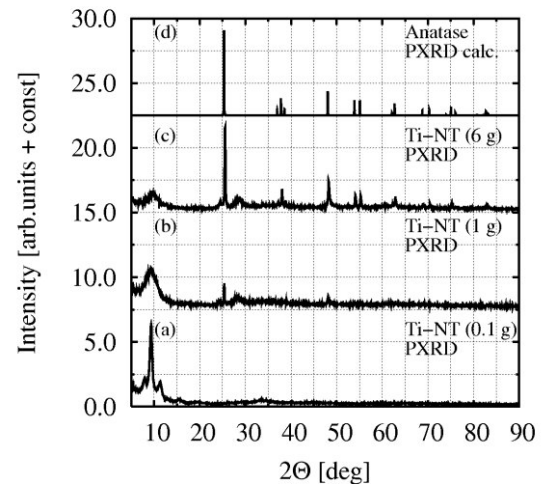


Figure 2. Ti-NT synthesized from different concentration of TiO_2 : (a) 0.1 g of mA per 100 ml (b) 1 g of mA per 100 ml, (c) 6 g of mA per 100 ml; (d) is the calculated PXRD pattern of anatase. Note successive decrease in intensity of anatase diffractions with decreasing mA concentration.

Ti-NT prepared from nanopowders (Fig. 4c,d). In case of nanopowder-based Ti-NT, the ED and PXRD were quite similar, showing three characteristic Ti-NT diffractions (at $24, 28$ and 48°). The other intensive peak in PXRD (at 10°) could not be observed at ED as it was hidden by beamstopper. In case of micropowder-based Ti-NT, the ED and PXRD diffraction patterns were very different. Our tentative explanation is as follows: In case of ED, the diffraction pattern had to be recorded from locations where the specimens were thin enough to be transparent for electrons. In such places the specimens contained single nanotubes and, as a result, all ED diffraction patterns are the same. In case of PXRD, the diffraction patterns were re-

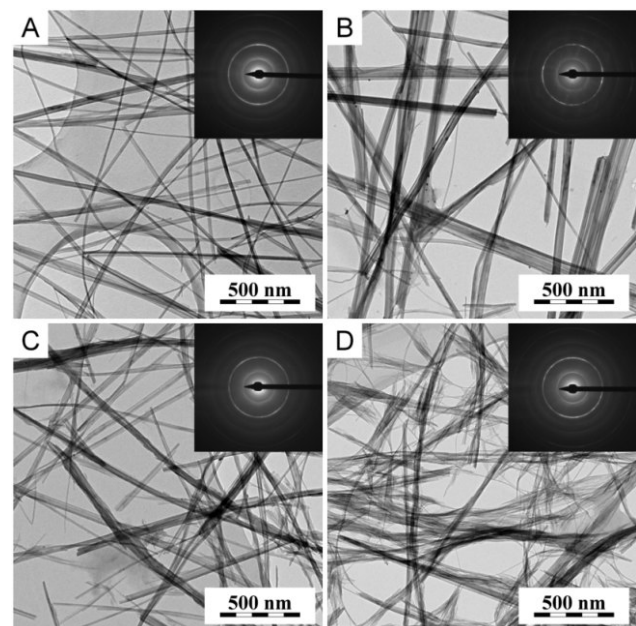


Figure 3. Ti-NT synthesized from: (a) microanatase, (b) microrutile, (c) nanoanatase and (d) nanorutile. TEM micrographs showed different thickness and length of each type of nanotubes, ED patterns did not show any difference.

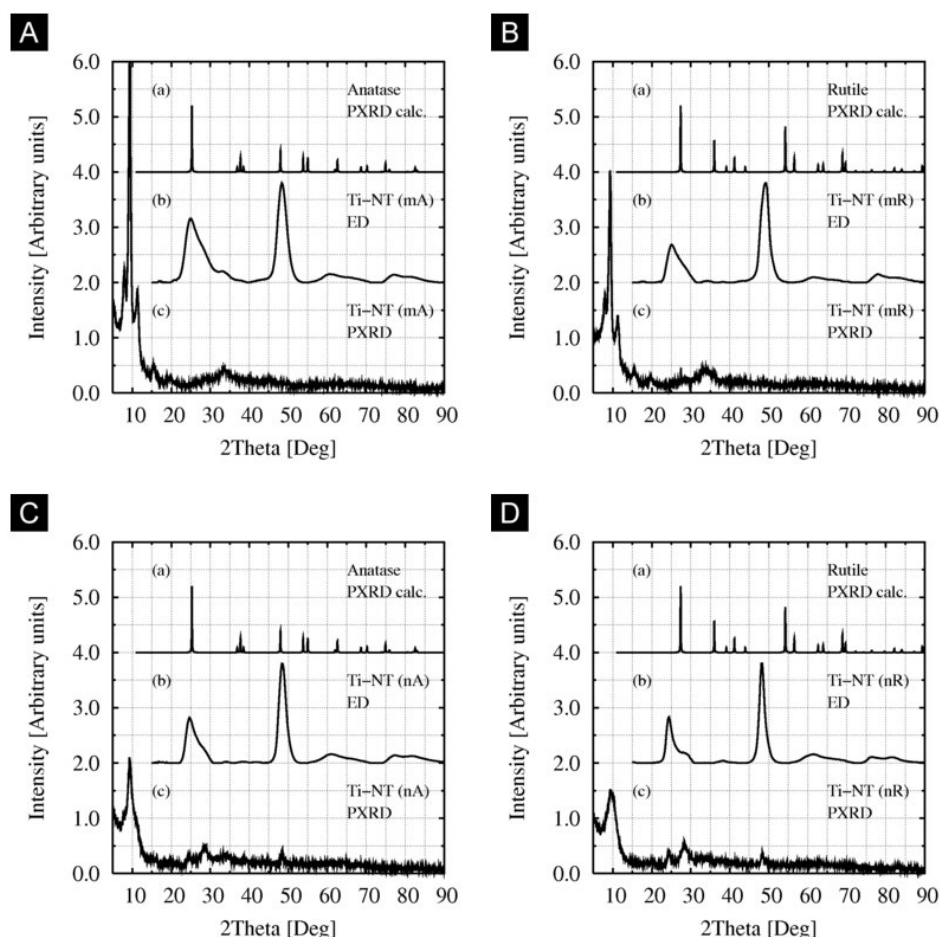


Figure 4. Influence of TiO_2 modification on Ti-NT crystalline structure. Comparison of calculated and experimental diffraction patterns of Ti-NT prepared from: (a) microanatase, (b) microrutile, (c) nanoanatase and (d) nanorutile. Single nanotubes always showed the same diffraction patterns (see ED in cases a,b,c,d), but larger agglomerates could be different (cf. PXRD in a,b and c,d).

corded from the whole specimens. Micropowder-based Ti-NT contained higher amount of nanotube agglomerates in comparison with nanopowder-based Ti-NT, which could be observed by SEM. The agglomerates had probably different crystalline structure (cf. Figs 4a-b and 4c-d). Moreover, the agglomerates were too big for ED (non-transparent for electrons) but their diffractions dominated in PXRD (much bigger crystallites). Consequently, the PXRD and ED patterns of micropowder-based Ti-NT were different.

Conclusion

Hydrothermal synthesis of Ti-NT, described in our previous work [8], was further investigated and optimized. Variable parameters during Ti-NT syntheses were: (a) initial concentrations of TiO_2 , (b) total reaction times, (c) average particle size of source TiO_2 powders and (d) crystalline modifications of source TiO_2 powders. Morphology of Ti-NT was investigated by both microscopic (SEM, TEM) and diffraction methods (ED, PXRD). The results could be summarized as follows: (i) *Residual TiO_2 particles* in final Ti-NT suspensions were eliminated by lower concentration of source TiO_2 powders (0.1 g per 100 ml of reactive mixture), together with longer reaction time (48 h). (ii) *Mor-*

phology of Ti-NT was just slightly influenced by source TiO_2 . Under the modified conditions (0.1 g TiO_2 , 48 h), all TiO_2 powders (anatase, rutile, micropowder, nanopowder) were completely transformed to Ti-NT, which were quite similar to each other, although the nanopowder of rutile seemed to yield the thinnest nanotubes. (iii) *Crystalline structure of single Ti-NT nanotubes* was essentially the same, as indicated by electron diffraction, whereas powder X-ray diffraction of the whole Ti-NT samples indicated that larger agglomerates of Ti-NT exhibited different crystalline structures.

References

1. Kasuga T., Hiramatsu M., Hodin A., Sekino T., Niihara K., Formation of Titanium Oxide Nanotube, *Langmuir* 1998; 14: 3160-3163.
2. Morgado Jr. E., de Abreu M. A. S., Pravia O. R. C., Marinkovic B. A., Jardim P. M., Rizzo F. C., Araújo A. S., A study on the structure and thermal stability of titanate nanotubes as a function of sodium content, *Solid State Sciences* 2006; 8: 888-900.
3. Tsai C.-C., Teng H., Structural Features of Nanotubes Synthesized from NaOH Treatment on TiO_2 with Different Post-Treatments, *Chem. Mater.* 2006; 18: 367-373.



4. Ma R., Bando Y., Sasaki T., Nanotubes of lepidocrocite titanates, *Chemical Physics Letters* 2003; **380**: 577–582.
5. Yao B.D., Chan Y.F., Zhang X.Y., Zhang W.F., Yang Z.Y., Wang N., Formation mechanism of TiO₂ nanotubes, *Applied Physics Letters* 2003; **82** (2): 281–283.
6. Wang W., Varghese O.K., Paulose M., Grimes C.A., A study on the growth and structure of titania nanotubes, *J. Mater. Res.* 2004; **19** (2): 417–422.
7. Weia M., Konishia Y., Zhoua H., Sugiharaa H., Arakawa H., Formation of nanotubes TiO₂ from layered titanate particles by a soft chemical process, *Solid State Communications* 2005; **133**: 493–497.
8. Králová D., Pavlova E., Šlouf M., Kužel R., Preparation and structure of titanate nanotubes, *Materials Structure* 2008; **15** (1): 41–45.
9. <http://www.ccp14.ac.uk/tutorial/powdcell/index.html>.
10. J. L. Lábár, *Microscopy and Analysis*, **75** (2002) 9–11.

The authors are indebted for financial support through grants MSMT 2B06096 (Ministry of Education, Youth and Sports of the Czech Republic), GACR 203/07/0717 (Grant Agency of the Czech Republic) and GACR 106/06/0761 (Grant Agency of the Czech Republic). MŠ acknowledges the participation in the EU Net work of Excellence Nanostructured Multifunctional Polymer Based Materials and Nanocomposites (NANOFUN-POLY).